# ON THE INTERPLAY BETWEEN ROTATION, DEFORMATION AND PAIRING

Ragnar Bengtsson, Ingemar Ragnarsson
Department of Mathematical Physics, Lund Institute of Technology, Box 725, S-220 07 Lund 7, Sweden.

Jing-ye Zhang*
Niels-Bohr Institute, Blegdamsvej 17, DK-2100 Copenhagen Ø, Denmark

and

Sven Åberg**
NORDITA, Blegdamsvej 17, DK-2100 Copenhagen Ø, Denmark

## Abstract

The influence of angular momentum on the extension of deformed regions is studied. Techniques based on the similarity between pairing rotational bands and ordinary rotational bands are used. Indications for an increase of deformation with increasing spin is obtained for rare-earth nuclei with neutron numbers N = 88-90. The yrast states of odd and even nuclei and of positive and negative parity are compared on an absolute scale. It is found that, in the rare-earth region, the odd-even energy difference has almost disappeared for I $\gtrsim$ 14. However, by considering both positive- and negative-parity yrast states, it is concluded that a substantial pairing gap exists also at higher spins.

## 1. Introduction

In the study of nuclei far from stability, different regions of deformation have attached a great interest. However, these investigations have mainly been limited to the ground state or the low-spin states. Recently, it has been possible to follow a large number of nuclei up to quite high-spin states, I = 20-30 or even higher. In the words of Bohr and Mottelson[1]), this opens a new dimension in our study of nuclei and it becomes possible to map out the regions of deformation, not only as functions of neutron and proton number but also as functions of angular momentum. Recent theoretical studies suggest that at very high angular momenta, almost all nuclei become strongly deformed. This is simply a consequence of the centrifugal foces as was first quantitatively accounted for in ref. [2]). In the present study, we will consider lower spins where the macroscopic centrifugal forces are of minor importance. For such spins, say I = 10-30 for nuclei with A ~ 150, it is mainly single-particle effects which are important. Our studies are thus strongly related to the change of the shell effects with angular momentum. Are there any new structures which can be observed at these angular momenta? Another question is what happens to the pairing energies with increasing spin. At which spin do the pairing correlations disappear[3])? Is it possible to observe any odd-even mass difference also at high spin?

Let us start by a more qualitative discussion in an attempt to clarify and relate some of the methods we will use (see also ref. [4])). In the rare-earth region, pairing is of great importance and in analogy with the quadrupole degree of freedom, one may say that the rare-earth region is well-deformed with respect to pairing. One then also talks about pairing-rotational bands (rotational bands in gauge space). Such a band is essentially the energy of a series of isotopes or isotones as illustrated schematically in fig. 1. For a pairing-rotational band, the energy E varies as $N^2$, N being the number of particles, in a similar way as the variation with $I^2$ for an ordinary rotational band. When the pairing correlations are strong, the local fluctuations are smeared out and the Fermi energy $\lambda$ is proportional to N. Furthermore, $\lambda$ is defined as $\lambda = \frac{\partial E}{\partial N}$. Thus, $\frac{\partial E}{\partial N} \propto N$ which leads to $E \propto N^2$ as stated above. The particle number N can be referred to as angular momentum in gauge space. The Fermi energy $\lambda$ then corresponds to the rotational frequency in ordinary space, $\omega$. The analogy can be put on a mathematically firm basis (see e.g. refs. [5,6])) and has consequences for example on two-particle transfer which have been experimentally tested.

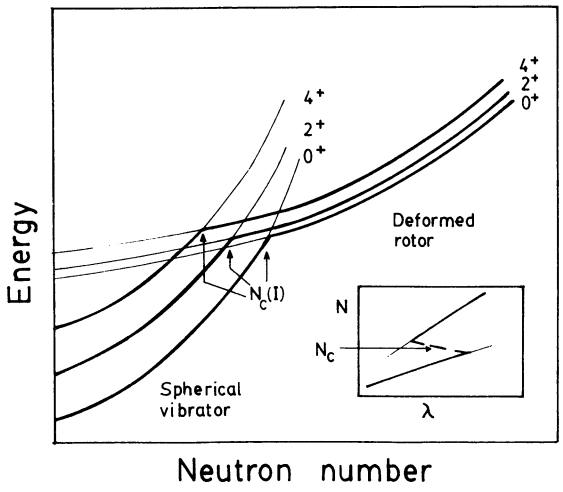


Fig. 1. Schematic illustration of pairing-rotational bands for spherical and deformed shape. With typical energy spacings, the deformed region appears to become larger with increasing spin. The inset shows that the shape transition is expected to manifest itself as a back-bend in an N vs. $\lambda$ diagram. The Fermi energy $\lambda$ is obtained as $\lambda = \frac{\partial E}{\partial N}$.

In fig. 1 is illustrated schematically how one pairing-rotational band is formed for spherical shape and another for deformed shape. If the transition was as sudden as

*) On leave of absence from Modern Physics Institute, Lanchow, China.
**) On leave of absence from Department of Mathematical Physics, Lund.

shown in the figure, it would lead to an abrupt change in the derivative $\frac{\partial E}{\partial N} = \lambda$. In a plot of N vs. $\lambda$, this would show up as a very pronounced back-bend at the critical particle number, $N_c$, where the transition occurs (see fig. 1, inset). The analogy to conventional back-bending plots, which can for example be drawn as $I=I(\omega)$, is obvious. It should also be mentioned that plots of $\lambda$ as a function of N are often used to identify ground-state shape transitions. However, $\lambda$ or rather $2\lambda$ is then generally referred to as the two-particle separation energy.

Pairing-rotational bands can also be drawn for non-zero angular momenta. In the spherical region, the low-angular momentum states are generally obtained from vibrational excitations of the nucleus. These excitations are approximately equally spaced in energy with a typical spacing of 600 keV in the rare-earth region. In the well-deformed region, rotational motion takes over and the excitation energies follow the $AI(I+1)$ systematics with $A \simeq 15$ keV. This means that for the excited pairing-rotational bands in fig. 1 a gradual decrease of $N_c$ with increasing spin is observed. From these oversimplified but general arguments one may expect an increase of the deformed regions with increasing spin. In practice, this may be seen for a transitional nucleus, being mainly vibrational at low spins and becoming more rotational at higher spins.

In sect. 2, we study the experimental shell energy vs. neutron number in realistic cases using plots similar to fig. 1. However, the evaluation of the shell energy requires that a macroscopic liquid-drop energy is subtracted and thus involves some arbitrariness. The model independent method of the inset in fig. 1 is therefore employed as an alternative in sect. 3. This method furthermore has the advantage to magnify the irregularities at a shape transition. The results obtained in sects. 2 and 3 may be put together in diagrams showing the different phases, defined by shape, particle alignment etc., which nuclei undergo with varying particle number and spin (sect. 4). In sect. 5 we concentrate on the single-particle excitations. The quasiparticle energies in the rotating frame are studied both as functions of rotational frequency in ordinary space ($\omega$) and in gauge space ($\lambda$). One important purpose of these single-particle studies is to find out what the observed spectra could tell about the disappearance of pairing at high spin. In this connection we also study the odd-even mass-difference as a function of spin.

## 2. Shell energies from experimental masses and excitation energies

For the Dy-nuclei, both masses and spectra up to high spins are known for a long chain of nuclei down to the very neutron deficient ones. Furthermore, the lightest isotopes with N around 82 are clearly spherical, those with N = 88-90 are transitional and the heaviest ones with N = 98-100 are strongly deformed. In fig. 2 we plot the energy in a similar way as in fig. 1. However, to make the variation anticipated in fig. 1 visible, the liquid-drop energy for spherical shape has been subtracted leaving what is generally referred to as the experimental shell correction. The yrast-spectra up to a maximum spin of 18 are then also plotted on top of the experimental shell corrections. For the liquid-drop energy, we have used the recent formula of Möller and Nix[7]) which seems to describe also nuclei far from stability with a high accuracy. However, other formula would lead to the same general appearance of the figure which thus can be considered as arising primarily from experimental data.

The curve for the ground state in fig. 2 is well-known. For N=82, the nucleus is spherical with a negative shell energy. With increasing neutron number away from N=82, the shell energy then increases and becomes positive. If the nuclei had stayed spherical, the shell energy would increase to a maximum somewhere in the middle between the magic numbers N=82 and N=126 and then decrease to a new minimum at N=126. However, long before this maximum is reached, it becomes more favourable for the nuclei to go deformed; a band-crossing in the language of fig. 1. The shell energy then flattens out or generally even begins to decrease because of shell effects for the deformed shape. For the Dy-isotopes, the maximum in the spin-zero curve is observed at $N \approx 90$ which is thus the transition point from spherical to deformed shape.

The way we plot the yrast bands in fig. 2 makes it possible to see, in a similar way as for the ground state, the transition point from spherical to deformed shape also for the higher spin states. One observes that with increasing spin, the maximum moves towards a smaller neutron number. Thus, for $^{154}_{66}Dy_{88}$, the low-spin states are expected to be of vibrational type but a transition to rotational motion appears to occur somewhere around I=6. As was discussed in the introduction (see fig. 1), the enlargement of the deformed region is easy to understand from the lower excitation energies in the rotational than in the vibrational bands. It is, however,only up to spins 10-14 that this enlargement is expected. Higher spins are for all nuclei formed from configurations involving p-h excitations in which case no systematic difference between spherical and deformed nuclei is expected. This is also what comes out from the Dy-isotopes where for spins between 10 and 20 the maximum stays between N=87 and 88. The small fluctuations are mainly due to irregular structure of the yrast spectrum of $^{152}$Dy which is known to be built from p-h excitations. Let us also mention that at somewhat higher spins we expect another enlargement of the deformed regions. The mechanism behind is, however, different and can be understood from the classical centrifugal forces as mentioned in the introduction.

The overall impression from fig. 2 is that the general structure is very stable with increasing spin. Thus for spins up to at least 20 the shell effects appear to be very similar to those of the ground state. Away from the critical neutron number $N_c$, the transition from the ground to the S-band

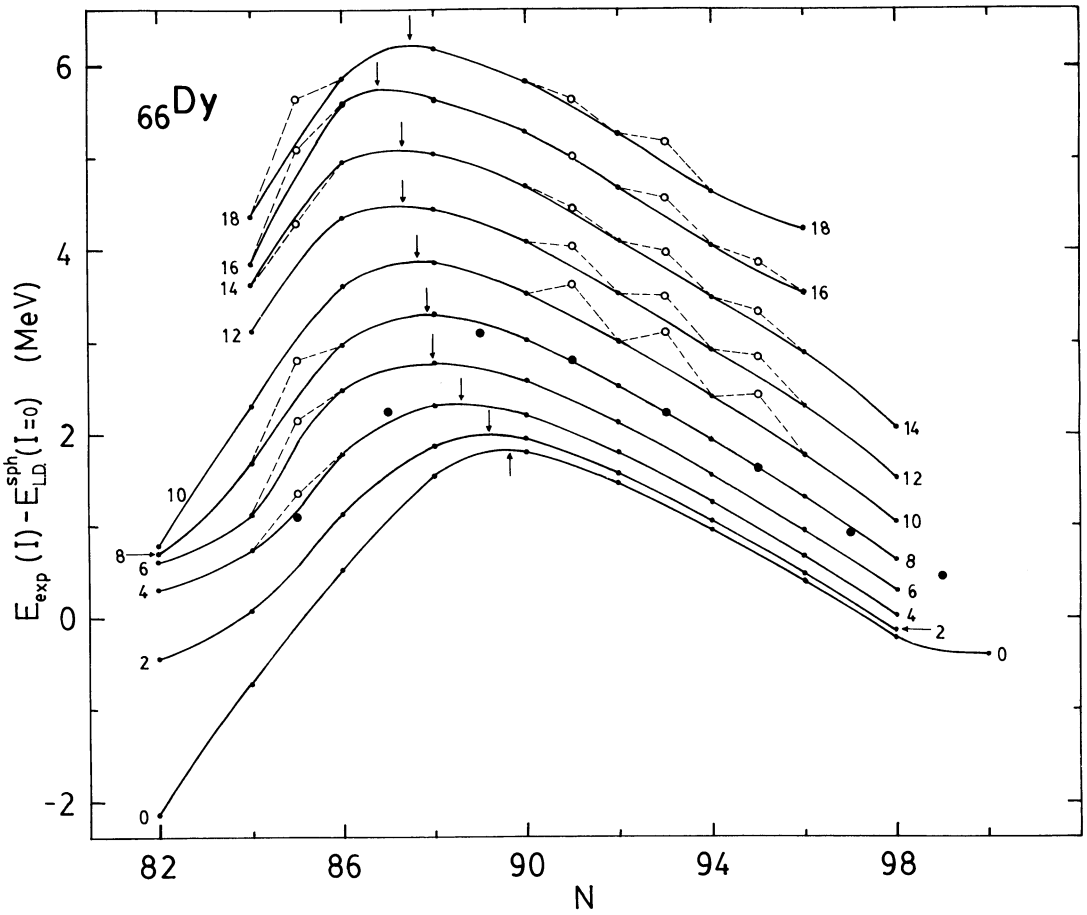


Fig. 2. The yrast levels for I = 0-18 of $_{66}$Dy plotted relative to the liquid-drop energy for spherical shape. The experimental masses are taken from refs. [8,9]) and the excitation energies from ref. [10]). The arrows indicate the maxima, which should roughly correspond to the shape transition. For odd nuclei, we indicate the ground-state energies by filled circles and some higher spin states by open circles. The energy of for example I=10 for an odd nucleus is obtained as the mean value of the I = 19/2 and I = 21/2 yrast energies. The fact that almost no odd-even mass difference is observed for I $\gtrsim$ 14 does not imply that the pairing gap is zero.

is seen only as a small disturbance on the character of the yrast spectra. This disturbance is far from changing the fact that,at least for N $\geq$ 90,the nuclei are deformed and rotate in a collective way, while for N $\leq$ 86 the spin is built from p-h excitations at no or small deformation. In the transitional region, however, such small disturbances might have a rather drastic effect on the yrast spectra. Note also that for spins I = 10-20, the nucleus $^{152}_{66}Dy_{86}$ is energetically very close to getting deformed with collective rotation.

The experimental shell energies for some odd nuclei are also shown in fig. 2. For the ground states, the odd-even mass differences are clearly seen. The excitation energies of the higher spin states are plotted as the mean values of the I - 1/2 and I + 1/2 yrast energies where I = ... 10, 12, 14, 16, ... . This makes the comparison to the even nuclei straight-forward. It is interesting to observe that at spin 10, most of the odd-even mass difference has disappeared and that very little of this difference is left for higher spins. This seems rather natural, because when the even nucleus begins to break pairs it should be similar to an odd nucleus (cf. sect. 5 below). It is also consistent with the fact that for N $\approx$ 85, the odd-even mass difference disappears at even lower spins because for the surrounding even nuclei, already the low-spin states are more or less pure particle-hole excitations. Observe, however, that even if the odd-even mass difference disappears at a rather low spin, it does not mean that the pairing gap,$\Delta$,is zero for this spin.

The ground-state experimental shell energies of the $_{40}$Zr-isotopes are exhibited in fig. 3. Also shown are the known excitation energies of the yrast $2^+$ and $4^+$ states. The mass for $^{102}$Zr is not known so here we have used a calculated value [7]). This mass is however not important for our discussion below but makes the figure somewhat more clear.

For the ground state we observe in addition to the expected shell-energy minimum at N=50 also a second irregularity at N=56. For this latter neutron number, the shell energy is 500-600 keV lower than would be

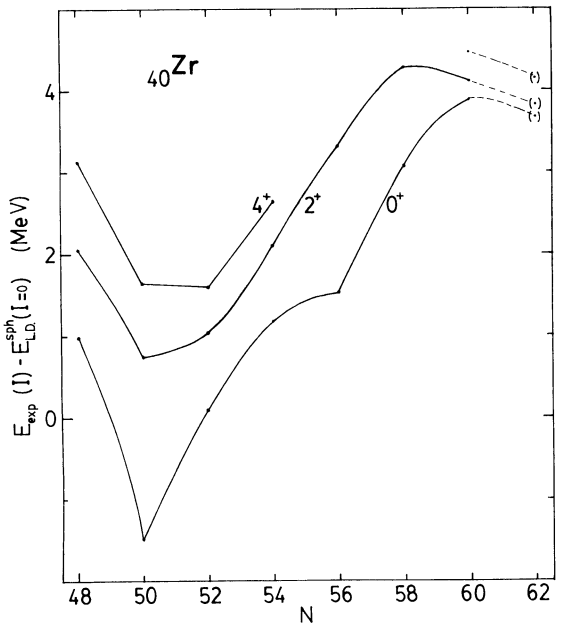


Fig. 3. Yrast energies of the Zr-isotopes plotted in a similar way as for the Dy-isotopes in fig. 2. The mass of $^{102}_{40}Zr_{62}$ has not been measured and is taken from calculations. Note the low $0^+$ state for N=56 while the corresponding $2^+$ state fits the systematics of neighbouring isotopes.

expected from the trend of neighbouring even nuclei. The low value for $^{96}$Zr has earlier been discussed (see e.g. [11])) and is clearly associated with the sub-shell closure at N=56. It is,however,interesting to observe that for the $2^+$ state, the irregularity at N=56 has disappeared and a smooth trend is observed. Thus, in $^{96}$Zr it seems more appropriate to state that the $0^+$ state is unusually low than that the $2^+$ state is unusually high. Going away from the $^{96}$Zr ground state, not in spin but instead in neutron number, one notes again that the strong binding at N=56 disappears. The strong binding of $^{96}$Zr thus seems to be associated with the combination of the subshell closure at Z=40 and N=56. As soon as one of these subshells is broken, either from particle-hole excitations or from addition or removal of particles, the extra binding disappears.

In fig. 3, one also observes how the Zr-isotopes get deformed around N=60. If only the measured masses ($N \leq 60$) are considered this does not show up for the ground state but quite clearly for the $2^+$ states. This is so because, in a similar way as for the Dy-isotopes, the transition to deformed shapes seems to occur at a lower neutron number for the $2^+$ states than for the ground states.

## 3. Back-bending in gauge space

The analogy between the three-dimensional ordinary space and the two-dimensional gauge space was pointed out in the introduction. For the study of shape transitions, one may therefore directly adopt the experience obtained from the study of irregularities in ordinary rotational bands. Such irregularities are conventionally magnified in back-bending plots showing the angular momentum (or moment of inertia) as a function of the rotational frequency. The analogous plot in gauge space is the particle number N versus the Fermi energy $\lambda$ as discussed in the introduction.

In fig. 4, we exhibit a plot of calculated N-values vs. $\lambda$ for two fixed deformations, $\varepsilon=0$ and $\varepsilon=0.25$, respectively. The $\lambda$-values have been obtained from the BCS-equations which were applied to the Nilsson model orbitals. One observes that around N=82, the marginal energy cost to add one additional neutron, $\frac{\partial E}{\partial N} = \lambda_n$, is about equal for spherical and deformed shape while for higher particle numbers the energy cost is largest for spherical shape. However, it is first for $N \approx 88$ that the total energy becomes lower for deformed than for spherical shape. With the reasonable assumption that $^{152}Dy_{86}$ is spherical, $^{154}Dy_{88}$ is transitional and $^{156}Dy_{90}$ is clearly deformed,the back-bend would show up as indicated by the dashed line in fig. 4.

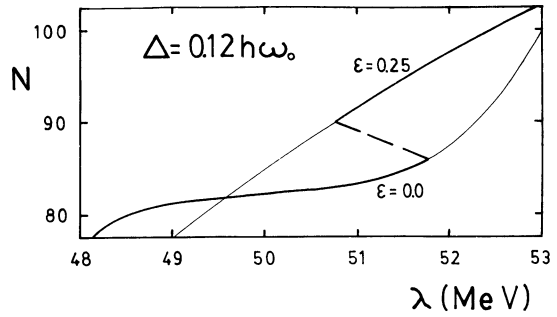


Fig. 4. Calculated neutron numbers, N, vs. Fermi energies $\lambda$ for spherical shape, $\varepsilon=0$, and deformed shape, $\varepsilon=0.25$. The Fermi energies were calculated from standard Nilsson model single-particle energies and a BCS-code. The back-bend,which would arise from the reasonable assumption that the nucleus is spherical for N=86, transitional for N=88 and deformed for N=90,is indicated.

The analogy between properties in gauge space and in ordinary space can be seen in the Cranking Hartree-Fock Bogolyubov (CHFB)-formalism. Using the mean field approximation for the quadrupole as well as the pairing field, one obtains the CHFB-Hamiltonian:

$$H' = H_o - \varepsilon\hat{Q} - \Delta(\hat{P}^+ + \hat{P}) - \lambda\hat{N} - \omega\hat{I}_x \qquad (1)$$

The notations used in this equation should be self-explanatory. In a similar way as the quadrupole field may break the spherical symmetry in ordinary space, the pair field may break this symmetry in gauge space. Thus the two Lagrangian multipliers, $\lambda$ and $\omega$, enter on the same footing. They can both be derived from experimental energies, namely

$$\lambda_p(Z,N,I,\nu) = \frac{\partial E(Z,N,I,\nu)}{\partial Z} \approx \frac{E(Z+1,N,I,\nu)-E(Z-1,N,I,\nu)}{2} \qquad (2)$$

$$\lambda_n(Z,N,I,\nu) = \frac{\partial E(Z,N,I,\nu)}{\partial N} \approx \frac{E(Z,N+1,I,\nu)-E(Z,N-1,I,\nu)}{2} \qquad (3)$$

$$\omega(Z,N,I,\nu) = \frac{\partial E(Z,N,I,\nu)}{\partial I_x} \approx \frac{E(Z,N,I+1,\nu)-E(Z,N,I-1,\nu)}{I_x(I+1)-I_x(I-1)} \quad (4)$$

where we have distinguished between the neutron and the proton Fermi energies. The nuclear energy of a state with angular momentum I and the additional quantum numbers $\nu$ is defined as

$$E(Z,N,I,\nu) = -E_B(Z,N)+E_{ex}(Z,N,I,\nu) \quad (5)$$

where $E_B(Z,N)$ is the ground state binding energy and $E_{ex}(Z,N,I,\nu)$ is the excitation energy relative to the ground state.

We have applied the equations above to the yrast states of the Dy-isotopes. Thus, N is plotted as a function of $\lambda_n$ in fig. 5. In agreement with fig. 2, a strong irregularity appears around neutron number 88 at spin zero. For higher spins we observe a similar irregularity but now at lower neutron numbers. As was discussed above, this irregularity is connected with a shape transition from near-spherical shape at lower N-values to well-deformed shape at higher N-values. The curve corresponding to the spherical liquid drop is also shown in fig. 5.

The experimental shell-correction energy in fig. 2 was defined as

$$E_{exp}^{shell}(Z,N,I,\nu) = E_{exp}(Z,N,I,\nu)-E_{L.D.}^{sph}(Z,N) \quad (6)$$

At the maximum points in fig. 2

$$\frac{\partial E_{exp}^{shell}(Z,N,I,\nu)}{\partial N} = 0. \quad (7)$$

It therefore follows immediately that the maxima in fig. 2 correspond to the points where the experimental curves are crossed by the liquid-drop curve in fig. 5. It is obvious that the crossing point with the liquid-drop curve does not exactly coincide with the inflexion point in the experimental $N(\lambda_n)$-curve. This is consistent with our general understanding of a shape transition as a smooth process with no really well-defined transition point.

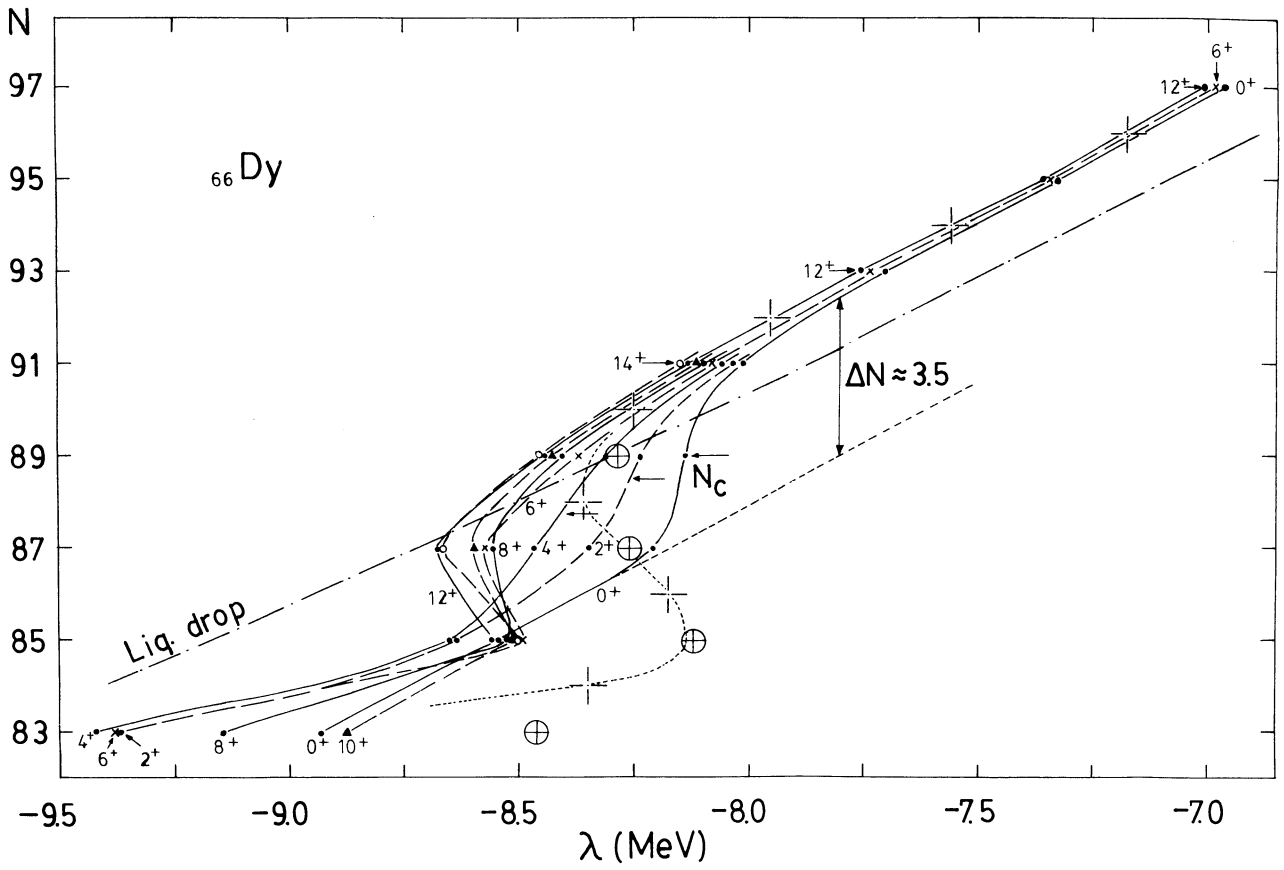


Fig. 5. Neutron number N vs. Fermi energy $\lambda$ for even Dy-isotopes. The values for angular momentum I = 0-14 are calculated from experimental masses and yrast spectra. It is indicated that, in analogy with angular momentum alignment, one can define a particle number alignment of $\Delta N=3.5$ for the Dy-isotopes. The figure also shows the behaviour of the spherical liquid drop[12]). The short-dashed line and the crosses give theoretical values of $\lambda$ calculated in a similar way as in fig. 4. The inflexion points, defining the N-values, $N_c(I)$, are indicated by arrows.

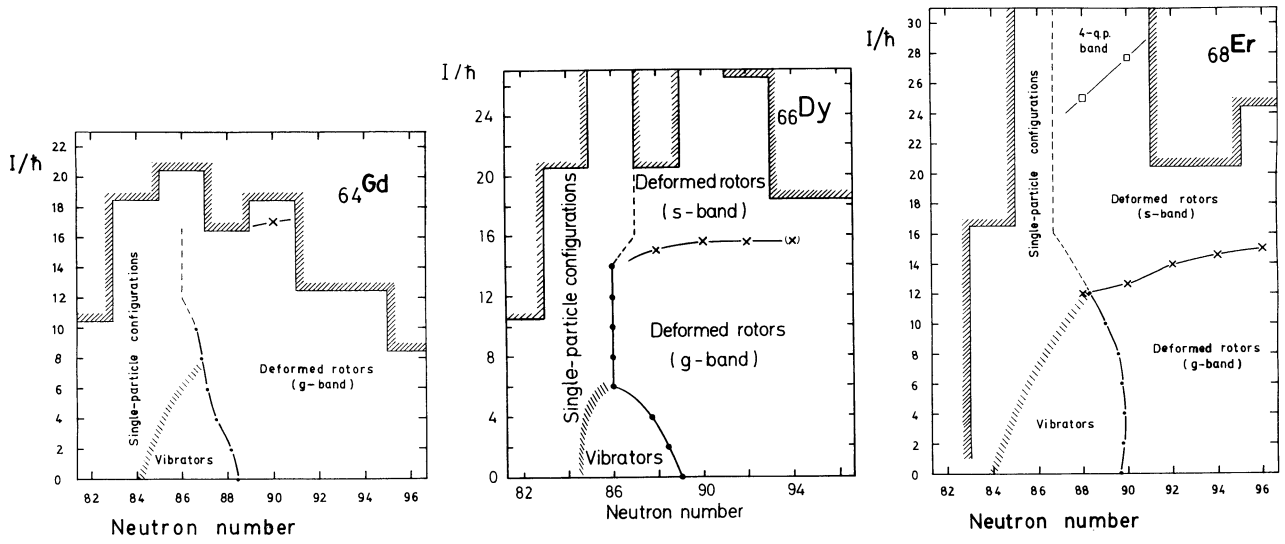


Fig. 6. Phase diagrams, obtained from experimental quantities, for even Gd, Dy and Er isotopes. The critical N-values of the shape transitions (points) are determined from N($\lambda$) plots (fig. 5) while the critical angular momentum, $I_c$, for the transition to two-quasiparticle (crosses) and four-quasiparticle bands (squares) are extracted from ordinary back-bending plots, I vs. $\omega$. Above the shadowed line, no experimental data are available. In many cases, the transition from one phase to another is not sharp but occurs gradually.

## 4. Phase diagrams

The critical neutron numbers, $N_c$, determined from the inflexion points in the N($\lambda_n$)-diagram can be summarized together with the critical angular momentum, $I_c$, determined from the $I_x(\omega)$ diagrams, in a phase diagram (fig. 6). Such a diagram, as introduced in refs. [13,14]), shows the different phases nuclei undergo with increasing angular momentum in ordinary space and in gauge space (the latter being the neutron number N). The interplay between these two types of "angular momenta" is thus nicely illustrated. In particular, one can read out at what neutron number the transition from near spherical to deformed shapes takes place. Thus for Dy we see a gradual decrease of $N_c$ (transition spherical-deformed), when going from I=0 to I ~ 6, as discussed in the introduction and in sect. 2.

Comparing the phase diagrams of $_{64}$Gd, $_{66}$Dy and $_{68}$Er (fig. 6), we observe the tendency that the $N_c$ values increase and the $I_c$ values (transition g-band - s-band) decrease when going from Gd to Er. The increase of $N_c$ indicates that the Gd-isotopes (in the region N $\gtrsim$ 88) are softer towards deformation than the Er-isotopes (cf. ref. [15])). The suggested smaller deformation in Er makes the orbitals easier to align (a larger slope in a plot like fig. 9) and thus leads to a decrease of $I_c$.

As shown in these phase diagrams, the shape of some special nuclei (e.g. N $\approx$ 88) will change from near spherical to well deformed along the yrast line. Such a shape transition may play an important role in causing back bending in ordinary space (see e.g. [16])).

A support for an increase of the deformation along the yrast line was recently obtained by a Risø-Oslo collaboration[17]). At low spins for the nucleus $^{157}_{67}Ho_{90}$ they observed a fairly large signature splitting. As the odd proton is in the orbital [523 7/2], originating from $h_{11/2}$, this requires a quite small deformation. Above the backbending, caused by the alignment of two $i_{13/2}$ neutrons, no signature splitting was observed in this $7/2^-$-band. A possible explanation is that the deformation has increased[17]). This interpretation of the data is consistent with the fact that when the same band is observed in heavier isotopes (with a large deformation), it does not show any signature splitting.

## 5. The pair field at high angular momentum

In sect. 2 we observed that most of the odd-even energy difference disappeared at angular momentum I ~ 14 when we compared energies of positive-parity states in Dy-isotopes. The high-spin yrast states of the odd-N isotopes belong to the $i_{13/2}$-band. In CHFB-calculations (sect. 3) of the quasiparticle levels as functions of the rotational frequency $\omega$ [18]), the levels of the $i_{13/2}$ high-j intruder shell penetrate into the pair gap already at low rotational frequencies. This explains why the energy of the $i_{13/2}$ bands do not reveal the existence of a pair field at high angular momentum. However, if we had plotted the energy of the negative-parity yrast states of the odd isotopes in fig. 2, we would have seen a significant odd-even energy difference up to the highest spins.

To illustrate the difference between the two parities, fig. 7 was prepared. We have considered the Yb-isotopes, which to

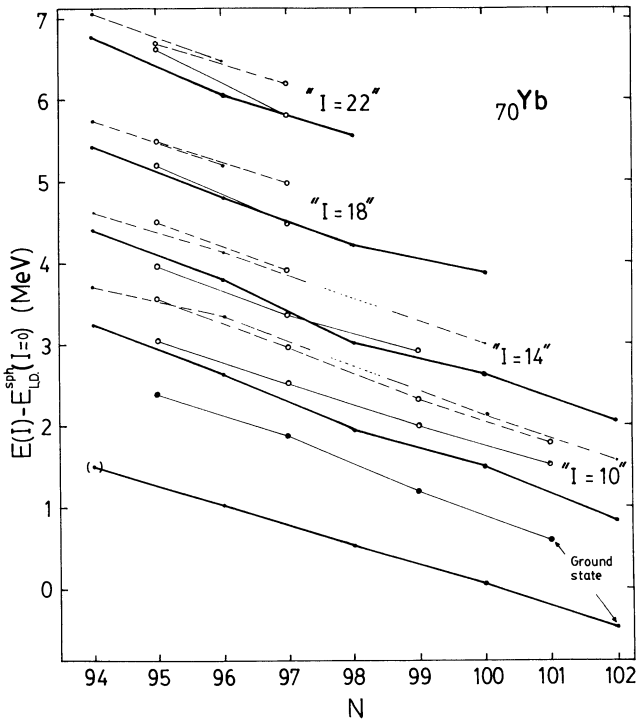


Fig. 7. Positive- and negative-parity yrast states for $_{70}$Yb drawn in a similar way as for $_{66}$Dy in fig. 2. For I=10, 14, 18 and 22 the lowest positive- (solid lines) as well as negative- (dashed lines) parity states are exhibited. For odd nuclei, the energy for even spin is defined from interpolations in the favoured band. This is also the case for negative parity in even nuclei if a band with odd spins is favoured. The high-spin spectrum is known also for lighter isotopes but the masses are not. Indeed, the mass for N=94 has been extrapolated from the heavier isotopes. Note that above spin 14, it is only the negative-parity states which reveal the existence of a pairing gap.

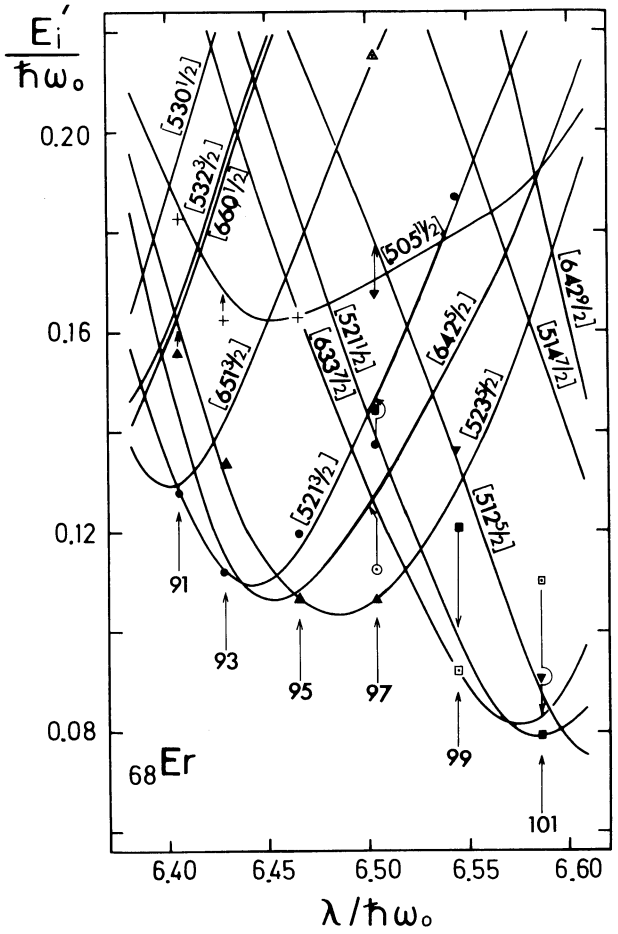


Fig. 8. Theoretical quasiparticle levels for Er at ω=0. The deformation and the pairing gap has been varied as a function of N as calculated for the ground states of the Er-isotopes[22]). Experimental band-head energies for a number - as we believe - relatively pure quasiparticle configurations in the odd-N isotopes are also included. The position of the experimental points has been adjusted in such a way that the ground state coincides with the corresponding theoretical level.

our knowledge are best known in the high-spin region[19-21]). The yrast levels are plotted in a similar way as in fig. 2. However, in fig. 7 the two parities have been treated independently. As expected, the $i_{13/2}$ positive-parity levels of the odd isotopes approximately coincide with the yrast spectra of the even isotopes for $I \gtrsim 14$. The negative-parity yrast states on the other hand, both for odd and even neutron numbers, come at a substantially higher energy all the way up to I=22. This seems to be connected with the fact that these states have one unpaired quasiparticle in a negative-parity orbital.

In order to understand this difference between the odd and the even parity states we have to investigate the quasiparticle spectrum at high frequencies. However, it may be useful to first discuss a couple of simpler cases, like the quasiparticle levels in non-rotating nuclei. Thus, fig. 8 shows the quasi-particle energies, $E'_i = \sqrt{(e_i-\lambda)^2+\Delta^2}$, as functions of the Fermi energy, $\lambda$. The energies of the single-particle levels are denoted by $e_i$. The deformation $(\varepsilon,\varepsilon_4)$ and the pairing gap have been varied with $\lambda$ (or neutron number) to be realistic for the $_{68}$Er isotopes. In fig. 8 is also given the energies of some measured band heads. The good agreement between theory and experiment shows that these calculations can be considered as quite reliable.

The energies $E'_i$ of fig. 8 are obtained from the simple BCS-equations. When the nucleus rotates, the more involved CHFB-equation (sect. 3) must be used instead. The quasiparticle levels in the intrinsic system can then be calculated as functions of the rotational frequency, $\omega$ [18]). Such a figure is provided in fig. 9. In contrast to fig. 8, also the conjugate partner (the mirror image) of each quasiparticle is shown at a negative energy. Furthermore, the time-reversal symmetry is broken for $\omega \neq 0$ and each quasi-particle level splits up into two branches which can be distinguished by a new quantum number, the signature, which takes the values $\alpha = 1/2$ and $\alpha = -1/2$. At $\omega=0$, the energies of fig. 9 should, except for small parameter differences, coincide with the N=94 ($\lambda = 6.44\ \hbar\omega_0$) energies of fig. 8. With increasing $\omega$, we then see how the large pair gap gradually disappears when the quasi-particle levels dive down into the gap. There is, however, a clear difference between the (high-j) positive- and (low-j) negative-parity levels. Thus, the positive-parity levels ([642 5/2] at $\omega=0$ in fig. 9),

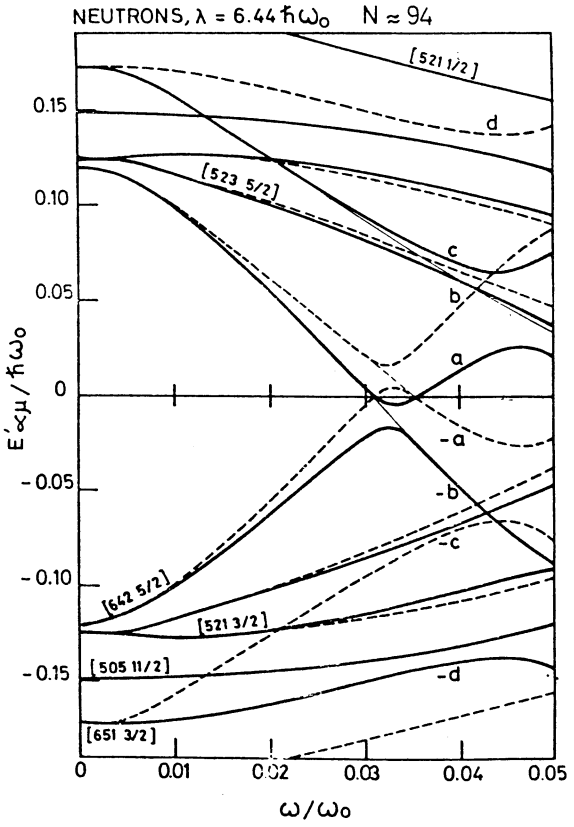


Fig. 9. Quasiparticle energies for neutrons plotted as functions of the rotational frequency ω. The deformation ($\varepsilon,\varepsilon_4$), the pairing gap Δ and the Fermi energy λ have been chosen to describe the ground state for $^{164}Yb_{94}$. For ω≠0, the time-reversal symmetry is broken and the levels split into two signatures which are distinguished by dashed and solid lines, respectively. For each pair of conjugate states, a label [$Nn_z\Lambda\Omega$] is indicated on either the level with positive energy or the one with negative energy, depending on whether the corresponding single-particle level (for ω=0) is situated above or below the Fermi surface.

reach the middle of the gap at $\omega/\omega_0 \simeq 0.03$ and then give rise to a back-bend when the two-quasiparticle state become yrast. However, no negative-parity quasiparticle energy comes close to zero in the frequency interval displayed in fig. 9 (the highest frequency $\omega/\omega_0 = 0.05$ corresponds roughly to angular momentum 30). Since the energy of the quasiparticle level occupied by the odd quasiparticle is equal to the excitation energy relative to the even-even vacuum, we can easily understand why the positive-parity yrast states in the odd-N nuclei do not show any significant energy difference as compared to the even-even yrast states above $\omega/\omega_0 \approx 0.03$ ($I \approx 14$), while the opposite is true for the negative-parity yrast states. This understanding is obtained with a fixed pairing gap and without considering blocking effects.

We are now prepared to investigate the quasiparticle energies for a fixed value of

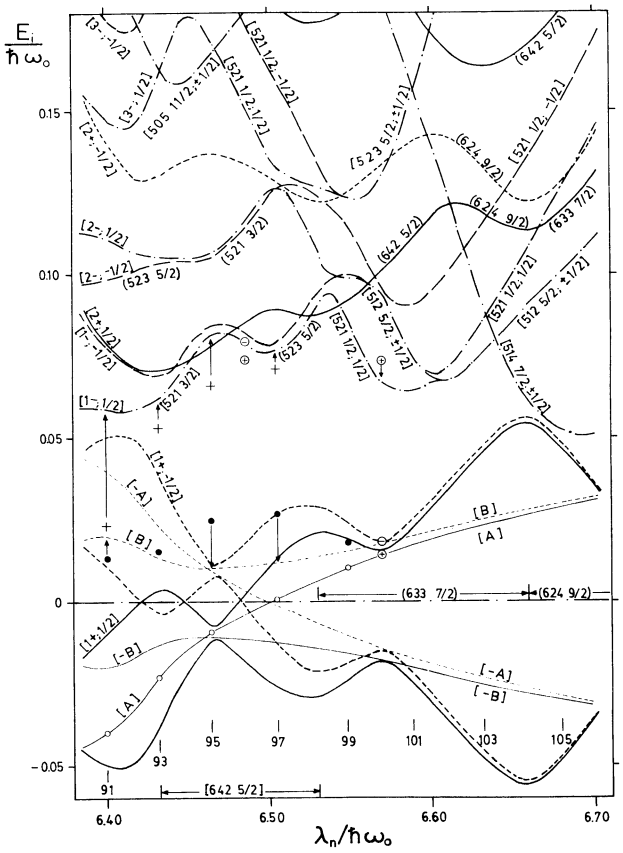


Fig. 10. Theoretical and experimental quasineutron energies for Yb-isotopes at a fixed rotational frequency, $\omega/\omega_0 = 0.03$ drawn as functions of the Fermi energy, λ (i.e. the rotational frequency in gauge space). The positive-parity levels are drawn with solid (signature, α=1/2) and short-dashed (α=-1/2) lines, the negative-parity levels with dot-dashed (α=1/2) and long-dashed (α=-1/2) lines. If a level has reasonably pure Nilsson labels, these are shown in square brackets [$Nn_z\Lambda\Omega$]; other levels are only labelled [νπ;α] where ν indicates the number of a level within its symmetry group, (π,α), counted from the Fermi surface and π is the parity. In some cases, Nilsson quantum numbers are given in round parenthesis, indicating the dominating component in the wave-function. The dominating component of the $i_{13/2}$ levels lying inside the gap is also indicated (for example [633 7/2] in the region $6.53 < \lambda/\hbar\omega_0 < 6.66$). The thin lines show the non-interacting $i_{13/2}$-levels. They are indicated with thin lines also in fig. 9. For odd nuclei, due to the blocking effect described in the text, it is these non-interacting levels which should be compared to experiment. The deformation has been varied in a similar way as in fig. 8 while the pairing gap is reduced by 20% relative to the experimental odd-even mass differences. This reduced pairing gap varies in the interval 0.10-0.12 $\hbar\omega_0$ for neutron numbers N=91-99 and decreases for larger neutron numbers to reach a value of ~ 0.06 $\hbar\omega_0$ for N=105. The neutron numbers are given in the bottom of the figure. The experimental energies are extracted from the observed bands and interpolated to $\omega/\omega_0 = 0.03$ (corresponding to $I \approx 10$-14). Encircled symbols are used for the even isotopes. When it is not obvious with which theoretical level an experimental point should be compared, this is shown by an arrow. The good agreement between theory and experiment suggests that the chosen pairing gap is approximately correct.

$\omega$ and drawn as functions of the Fermi energy $\lambda$. Such a diagram for $\omega = 0.03\ \omega_o$, roughly corresponding to the frequency of the first back-bend, is exhibited in fig. 10, where it is evident that the single-particle levels are mixed in a much more complicated way than in the non-rotating case (fig. 8). However, also for $\omega/\omega_o = 0.03$, one clearly observes a pairing gap, which survives for all particle numbers shown. It is only the high-j $i_{13/2}$ levels, denoted by [1+, -1/2] and [1+, 1/2], which penetrate deeply into this gap. Other orbitals like [514 7/2] and [521 1/2] which come from lower-j shells behave roughly as in the $\omega$=0 case (fig. 8).

It is interesting to observe that the difference between the two parities survive through all the particle numbers of fig. 10. However, with the Fermi level in the upper part of the $i_{13/2}$-shell, the positive-parity orbitals should become more difficult to align and thus more similar to the negative parity orbitals. This is also what comes out from the quasiparticle levels of fig. 10. One would thus expect that for the heavier isotopes the odd-even energy difference would remain to higher spins also for the positive-parity states in the odd isotopes. Furthermore, the general appearance of the I=10 states in fig. 7 appear to support this conclusion.

In the rotational case of fig. 10, the experimental energies must be interpolated from the observed states in the spin region I $\approx$ 10-14, see ref. [18]). Before comparing theoretical and experimental data in fig. 10, it is also necessary to understand how the presence of an excited quasiparticle in one of the lowest $i_{13/2}$-levels effects the interaction between the quasiparticle levels a and -b (or b and -a) of fig. 9, that is the so called blocking effect. Thus, in the favoured $i_{13/2}$-band the levels a and -b are both filled (the levels b and -a are empty), which means that the interaction at $\omega/\omega_o \approx$ 0.035 only mixes the wavefunctions of two occupied levels, leaving the total many-particle wavefunction unchanged. The experimental quasiparticle energies, will therefore behave as if there were no interaction, following the thin downsloping solid line in fig. 9, which is a theoretical reconstruction of the non-interacting quasiparticle level. When making comparisons with experimental quasiparticle energies one must therefore use the non-interacting quasiparticle levels, which are also included in fig. 10 as the thin lines [A], [B], [-A] and [-B].

The frequency at which the non-interacting quasiparticle levels cross depend on $\lambda$. At the frequency $\omega/\omega_o = 0.03$ used in fig. 10 we are below the crossing frequency for $\lambda > 6.46\ \hbar\omega_o$ and above the crossing frequency for $\lambda < 6.46\ \hbar\omega_o$. This increase of the crossing frequency with increasing $\lambda$ is a manifestation of the fact that the low-energy $i_{13/2}$-orbitals are more easy to align than those higher up in the shell. The strong oscillations in the quasiparticle levels [1+; 1/2], [1+; -1/2] and their conjugate partners is a result of the oscillating interaction matrix element at the first crossing that involves these levels[18,23]).

When comparing experimental and theoretical quasiparticle energies in fig. 10, we use the favoured $i_{13/2}$ band as a reference for the odd isotopes. Also the energies which can be extracted from the side-bands of even isotopes are given relative to the favoured $i_{13/2}$ level. This explains why one experimental point always coincide with the level [A] in fig. 10.

It is very satisfying that relative to level [A], the experimental quasiparticle energies show the same pattern as the theoretical ones. The negative-parity states are systematically pushed up in energy compared to the positive-parity states. This would not be the case in absence of pair correlations, since then the positive- and negative-parity states would alternate as the lowest states, when the single-particle levels cross each other. Furthermore, the good quantitative agreement between experiment and theory in fig. 10 indicates that, for one- and two-quasiparticle configurations in the vicinity of the backbending frequency, the gap parameter must be close to the one used in the calculation.

## 6. Summary and conclusion

In the present paper we have studied systematics of nuclear properties as a function of particle number and spin. Special emphasis was put on the question of shape transitions. The analogy between such transitions and the transition to for example two-quasiparticle states at high spin (back-bend in gauge space and in ordinary space, respectively) was pointed out. The variation with spin of the critical particle number, $N_c$, where the shape transition occurs was studied. Two methods were used to extract $N_c$ (sect. 2 and sect. 3). In sect. 2 we thus studied irregularities in the experimental shell energies. In sect. 3 these irregularities, manifesting the shape transition, were blown up in plots of the neutron number versus the Fermi energy.In sect. 4,all the information on $N_c$ and $I_c$ were put together in phase diagrams (fig. 6) to illustrate the interplay between rotation, deformation and pairing. We then studied the single-particle degree of freedom in some detail. The consequences of a pairing gap on the high-spin yrast spectrum was investigated.

The main conclusion of our study are:

i) The deformed regions appear to become larger with increasing spin. Transitional nuclei may thus be vibrational like at low spin and rotational at high spin (e.g. $^{152}_{64}Gd_{88}$, $^{154}_{66}Dy_{88}$ and $^{156}_{68}Er_{88}$).

ii) In the sequence of isotopes $_{64}Gd$, $_{66}Dy$ and $_{68}Er$, the Gd and Dy isotopes get deformed at a lower N-value than the Er isotopes. This is so in spite of the semimagic properties of $^{146}Gd$.

iii) A strong binding for the $0^+$ state of a nucleus may have disappeared already for $2^+$ state (fig. 3).

iv) In the rare-earth region, the odd-even energy difference has almost dis-

appeared for I $\gtrsim$ 14. However, if both positive- and negative-parity yrast states are considered, the existence of a substantial pairing gap also at high spin is revealed.

v) The systematics of low- and high-spin states as a function of particle number is well described by calculated quasi-particle energies.

Our studies could become more complete if the masses and yrast spectra were known over larger regions of neutron (or proton) number. For example, for the Yb-isotopes, the yrast spectra are quite well-known for the neutron-deficient isotopes with N=90-94 while the masses are not known. Similarly, if the masses were known for the neutron-deficient Hg-isotopes, we believe that some interesting results could be obtained with the present methods.

Fruitful discussions with and valuable comments from Ben Mottelson are deeply acknowledged. Ragnar Bengtsson and Ingemar Ragnarsson thank the Swedish Natural Science Research Council and Jing-ye Zhang thanks the Danish Ministry of Education for financial support. Jing-ye Zhang is grateful for excellent working conditions at NBI and for the hospitality of the Department of Mathematical Physics in Lund.

References

1) A. Bohr and B.R. Mottelson, Phys. Scripta 10A (1974) 13

2) S. Cohen, F. Plasil and W.J. Swiatecki, Ann. of Physics 82 (1974) 557

3) B.R. Mottelson and J.G. Valatin, Phys. Rev. Lett. 5 (1960) 511

4) R. Bengtsson, Jing-ye Zhang and S. Åberg, to be published

5) D.R. Bés and R.A. Broglia, Proc. Int. School of Physics, "Enrico Fermi", 1976, course LXIX, ed. A. Bohr and R.A. Broglia (North Holland, 1977) p. 55

6) A. Bohr, J.M. Leinaas and P. Minnhagen, Nordita preprint 1979/13

7) P. Möller and J.R. Nix, Nucl. Phys. A361 (1981) 117 and Nucl. Data, to appear

8) A.H. Wapstra and K. Bos, Atom. Data and Nucl. Data Tables 19 (1977) 177

9) J. Blomqvist, private communications

10) C.M. Lederer and V.S. Shirley, "Table of Isotopes" 7th Edition (1978)

11) I. Ragnarsson, Proc. 6th Int. Conf. on Atomic Masses and Fundamental Constants, East Lansing, Michigan, 1979, ed. J.A. Nolen and W. Benenson (Plenum Press, New York, 1980) p. 87

12) W.D. Myers and W.J. Swiatecki, Ark. Fys. 36 (1967) 343

13) Gong-ou Xu and Jing-ye Zhang, High Energ. Fortis et Nucl. Phys. (China) 3 (1979) 232

14) I. Ragnarsson, T. Bengtsson, G. Leander and S. Åberg, Nucl. Phys. A347 (1980) 287

15) I. Ragnarsson, A. Sobiczewski, R.K. Sheline, S.E. Larsson and B. Nerlo-Pomorska, Nucl. Phys. A233 (1974) 329

16) Gong-ou Xu and Jing-ye Zhang, Nucl. Phys. A303 (1980) 189

17) P.O. Tjøm et al., private communications

18) R. Bengtsson and S. Frauendorf, Nucl. Phys. A327 (1979) 139

19) P.M. Walker, S.R. Faber, W.H. Bentley, R.M. Ronningen and R.B. Firestone, Nucl. Phys. A343 (1980) 45.

20) P.M. Walker, W.H. Bentley, S.R. Faber, R.M. Ronningen, R.B. Firestone, F.M. Bernthal, J. Borggren, J. Pedersen and G. Sletten, Nucl. Phys., to appear

21) Lund-Risø coll., private communication through W. Walus.

22) R. Bengtsson, Journal de Phys. C10 (1980) 84

23) H.-B. Håkansson, Phys. Lett. 94B (1980) 288